

# Dual-emitter graphene glass fiber fabric for radiant heating

*Hao Yuan<sup>†</sup>, Hui Zhang<sup>‡</sup>, Kewen Huang<sup>†</sup>, Yi Cheng<sup>†</sup>, Kun Wang<sup>†</sup>, Shuting Cheng<sup>‡</sup>,  
Wenjuan Li<sup>†</sup>, Jun Jiang<sup>‡</sup>, Junliang Li<sup>†</sup>, Ce Tu<sup>‡</sup>, Xiaobai Wang<sup>§,\*</sup>, Yue Qi<sup>†,‡,\*</sup>, and  
Zhongfan Liu<sup>†,‡,\*</sup>*

<sup>†</sup> Center for Nanochemistry, Beijing Science and Engineering Center for Nanocarbons, Beijing National Laboratory for Molecular Sciences, College of Chemistry and Molecular Engineering, Peking University, Beijing 100871, China

<sup>‡</sup> Beijing Graphene Institute (BGI), Beijing 100095, China

<sup>‡</sup> State Key Laboratory of Heavy Oil Processing, College of Science, China University of Petroleum, Beijing 102249, China

<sup>§</sup> Department of Materials Application Research, AVIC Manufacturing Technology Institute, Beijing 100024, China

\*Address correspondence: [xiaobai\\_wang@yeah.net](mailto:xiaobai_wang@yeah.net); [qiyue-cnc@pku.edu.cn](mailto:qiyue-cnc@pku.edu.cn);

[zfliu@pku.edu.cn](mailto:zfliu@pku.edu.cn)

## Supplementary Note

### Calculation of theoretical emissivity for graphene with different layers.

Single-layer graphene is found to absorb ~2.3% of the incoming IR radiation, theoretically as well as experimentally. And graphene has a very low reflectivity, and most of the incident electromagnetic waves are found to be transmitted.<sup>1, 2</sup> Therefore, for 15 layers of graphene, the theoretical emissivity ( $\epsilon$ ) can be calculated by:

$$\epsilon = \alpha = 1 - (1 - 0.023)^{15} = 0.29$$

where  $\alpha$  is the absorptivity. For 60 layers of graphene, the theoretical emissivity can be calculated by:

$$\epsilon = \alpha = 1 - (1 - 0.023)^{60} = 0.75$$

**Table S1. Information of purchased commercial glass fiber**

<b>Textile weave</b>	<b>Plain weave</b>
<b>Content of SiO<sub>2</sub> (%)</b>	<b>99.92</b>
<b>Diameter (μm)</b>	<b>7</b>
<b>Linear density (tex)</b>	<b>195.1</b>

**Table S2. Comparisons between previously reported infrared radiation materials and GGF in this work**

<b>Material</b>	<b>Emissivity</b>	<b>Thickness</b>
Fe <sub>2</sub> O <sub>3</sub> <sup>3</sup>	0.78-0.80 (near-infrared)	60-100 μm

Ferrites <sup>4</sup>	0.74 (3-20 $\mu\text{m}$ at 800 $^{\circ}\text{C}$ )	120-150 $\mu\text{m}$
$\text{CeO}_2$ <sup>5</sup>	0.889 (8-14 $\mu\text{m}$ at 750 $^{\circ}\text{C}$ )	$\sim 80$ $\mu\text{m}$
$\text{MnO}_2$ and rare-earth oxide <sup>6</sup>	0.917 (2.5-25 $\mu\text{m}$ at 1000 $^{\circ}\text{C}$ )	150-200 $\mu\text{m}$
<b>GGF (This work)</b>	<b>0.92 (2.5-25 <math>\mu\text{m}</math> at 500 <math>^{\circ}\text{C}</math>)</b>	<b>5-20 nm</b>

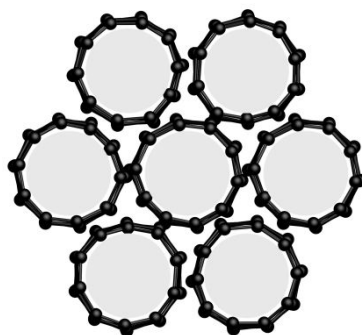


**Figure S1.** Simplified schematic of graphene glass fiber bundle.



**Figure S2.** Optical photograph of our self-developed batch production CVD equipment for GGF.

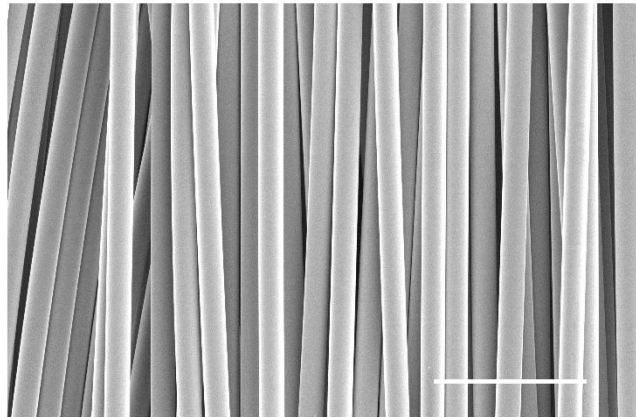


**Figure S3.** SEM image of GGF with well-retained microfiber profile. The fiber diameter is  $\sim 7 \mu\text{m}$ . Scale bar,  $50 \mu\text{m}$ .

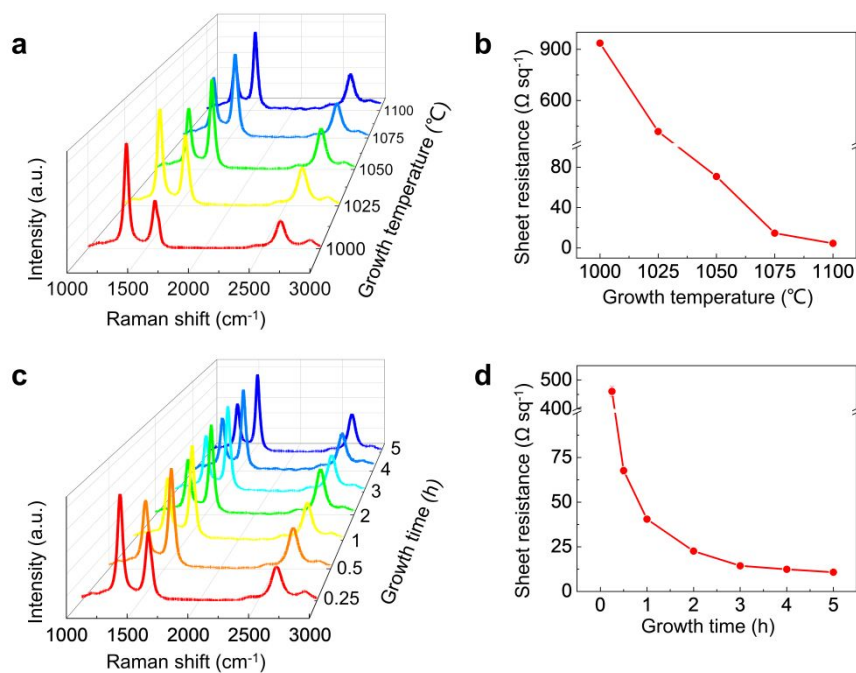


**Figure S4.** CVD growth of graphene on glass fiber. a,b) Temperature-dependent Raman spectra (a) and sheet resistance (b) of GGFF. c,d) Growth time-dependent Raman spectra (c) and sheet resistance (d) of GGFF.

**Other factors that can influence the graphene growth were systematically analyzed.**

**(1) Growth temperature of the CVD system.** Carbon source dissociation during the graphene CVD growth on the non-catalytic glass fiber mainly relies on the thermal decomposition. For CH<sub>4</sub> precursor, the C-H bond energy is very high (~4.85 eV), and the diffusion barrier of carbon atoms on oxide surfaces was found to be up to ~1 eV.<sup>7,8</sup> Therefore, the growth temperature of 1000 °C is not high enough for the full dissociation of CH<sub>4</sub> and the diffusion of active carbon species on glass fiber. Consequently, the growth rate and quality of graphene are limited (**Figure S4a**), resulting in a relatively low electrical conductivity (**Figure S4b**). As temperature increases, the quality of graphene was improved, and the improved thickness and quality also resulted in the higher electrical conductivity (**Figure S4a,b**). Therefore, in this CVD system, 1100 °C was chosen as graphene growth temperature.

(2) **Growth time of graphene in the CVD system.** CVD growth time is also a significant factor to modulate the thickness of graphene layers, and thus affect the sheet resistance. The carbon source decomposition mainly depends on pyrolysis on dielectric substrate, and the carbon precursors could keep dissociating even the substrate surface were fully covered with graphene, which is different from the self-limiting growth of graphene on copper substrate. As shown in the supplemented data in Figure S4c, as the growth time being extended, the graphene layers became thicker, which resulted in a lower sheet resistance (Figure S4d).

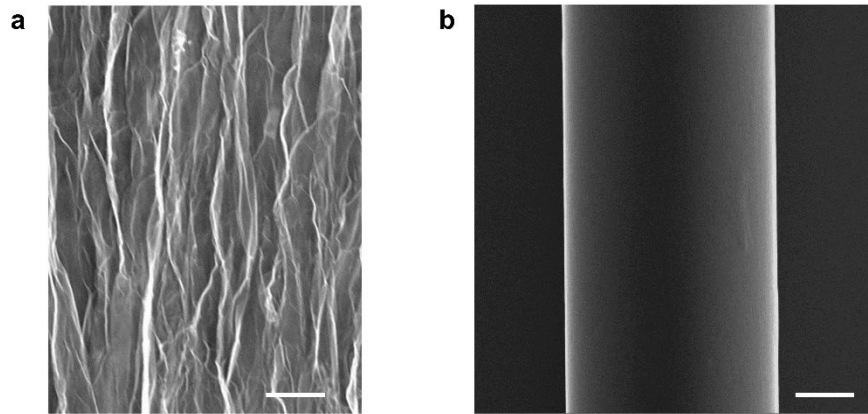


**Figure S5.** SEM images of a bundle of graphene ribbons (a) and single graphene ribbon (b) after etching the core glass fiber. Scale bars are 5  $\mu\text{m}$ .

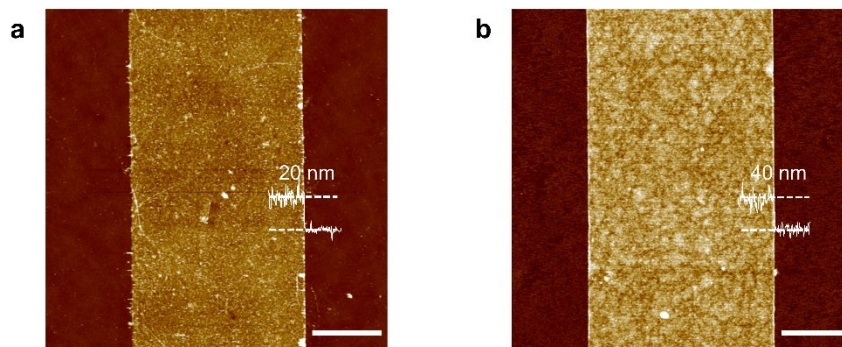


**Figure S6.** AFM images and corresponding thickness of graphene ribbons after etching the core glass fiber of GGFF-150 (a) and GGFF-30 (b) samples. Scale bars are 4  $\mu\text{m}$ .

After the core glass fiber was etched, the graphene shell was collapsed into a micro ribbon and the graphene covered above and below the glass fiber overlapped. Therefore, the height of graphene ribbon represents the thickness of overlapped graphene layers. The layer of graphene is calculated based on 0.33 nm per graphene layer.

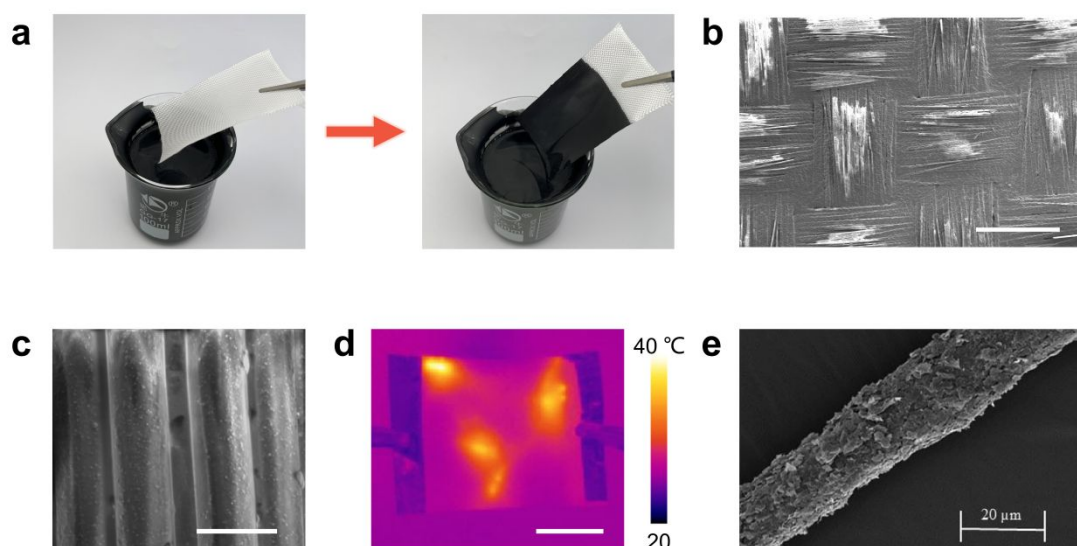


**Figure S7.** Graphene/glass fiber composite fabrication by coating graphene on glass fiber. a) Fabrication process of coating graphene on glass fiber by dipping. b,c) SEM images of graphene/glass fiber composite fabricated by coating graphene on glass fiber. Scale bars, 500  $\mu\text{m}$  (b), 10  $\mu\text{m}$  (c). d) Infrared image of graphene/glass fiber composite fabricated by coating graphene on glass fiber under input voltage of 100 V. Scale bar, 2 cm. e) SEM image of graphene/glass fiber composite fabricated by dipping in graphene-based conductive inks in literature<sup>9</sup>.

The direct depositions of graphene powder or graphene oxide on glass fibers or graphene/glass fiber composites are not new in this field. However, the graphene/glass

fiber composite obtained by simple physical coating instead of CVD growth usually showed limited performances in flexibility, interface stability, uniformity and electrical conductivity. The innovations of our system compared with the reported graphene oxide/glass fiber and graphene/glass fiber composites obtained through the coating deposition in the literatures have been systematically analyzed. In addition, the graphene/glass fiber composite by coating glass fiber in purchased commercial graphene-based slurry by ourselves was obtained. The fabrication process is illustrated in **Figure S7a**. The corresponding comparisons between graphene/glass fiber composite and GGFF developed in this work were shown in Figure S7.

(1) In this work, the full-surface, conformal growth of graphene on each glass fiber in the fabric was successfully achieved and the sheet resistance of the fabric showed high uniformity in the large-area GGFF (Figure 1h and S3). The experiments to coat the commercial graphene-based slurry directly on the surface of glass fiber to obtain graphene/glass fiber composite were carried out. Consequently, as shown in the SEM image of the coating samples (Figure S7b), it is hard to realize the uniform coating of graphene on the surface of glass fiber. The infrared image in Figure S7d presented the severe temperature non-uniformity when it was applied as electrothermal device. In addition, in reported literatures, the traditional method to combine graphene and glass fiber is repeatedly dipping glass fiber in graphene-based conductive inks<sup>9</sup> or graphene oxide (GO) dispersion. However, it is also a big challenge to realize the full surface, conformal and uniform graphene covering on the surface of each fiber (Figure S7e).

(2) For GGFF prepared in this work, the flexibility of glass fiber is well-retained because the as-grown graphene is only tens of nanometer, and the GGFF also shows strong interfacial stability between graphene and the fiber (Figure 4d,e). In contrast, the samples obtained by coating, the glass fiber is usually covered with thick graphene layers of several micrometers (Figure S7c), which largely degrades the intrinsic flexibility of the fiber, and the graphene coating layers also easily peel off fibers under bending or torsion due to the weak interfacial interaction between graphene and the fiber.

(3) Because of the high quality of CVD-grown graphene, the electrical conductivity of GGFF in this work can reach over  $2000 \text{ S m}^{-1}$ , and the sheet resistance is tunable from  $1\text{-}3000 \text{ } \Omega \text{ sq}^{-1}$ . The graphene-covered glass fiber fabric obtained by dipping in the graphene-based slurry presented the sheet resistance of  $\sim 20 \text{ k}\Omega$ , much higher than that of GGFF. For traditional method by coating graphene on glass fiber, to get a better electrical conductivity, the reduction process by chemical reduction or thermal reduction is usually needed. However, due to the low reduction degree of GO and low orientation degree of graphene sheets, graphene/glass fiber fabricated by coating always showed a low electrical conductivity (the electrical conductivity of graphene/glass fiber obtained in *J. Inorg. Mater.* 2015, 30, 763<sup>10</sup> is  $4.5 \text{ S m}^{-1}$ ).

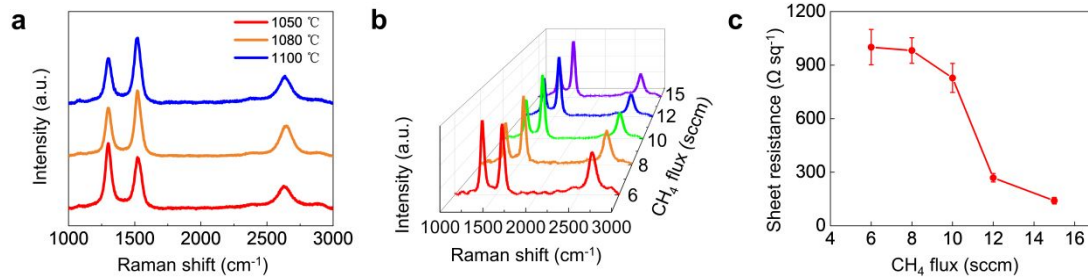


**Figure S8.** Graphene growth on ceramic fiber by CVD method. a,b) Raman spectra of CVD grown graphene at different temperature and  $\text{CH}_4$  flux, respectively. c)  $\text{CH}_4$  flux-dependent sheet resistance of graphene-covered ceramic fiber fabric.

The method developed in this work to combine graphene with glass fiber shows good compatibility with other fiber-shaped materials, such ceramic fiber, which have good high-temperature resistance and can withstand temperature over  $1000 \text{ }^\circ\text{C}$ .

The explorations about the combination of graphene with the ceramic fiber with the same method in this work were carried out. As shown in the Raman spectra in **Figure S8a,b**, graphene can be successfully synthesized on the ceramic fiber with the same CVD method, and the quality of graphene can be controlled by the modulating the growth parameters. The influences of growth temperature and  $\text{CH}_4$  flux on graphene quality grown on ceramic fiber were studied. The results showed that  $I_D/I_G$  in the Raman gradually decreased as the temperature increasing, indicating that the higher

temperature resulted in the higher quality of as-grown graphene (Figure S8a). With larger CH<sub>4</sub> flux, the graphene layer was thicker at the same growth time due to the sufficient supply of the active carbon species, and the higher growth rate of graphene (Figure S8b). In this way, by controlling the growth parameters, the sheet resistance of the graphene/ceramic fiber fabric can be modulated from 1-1000 Ω sq<sup>-1</sup> (Figure S8c).

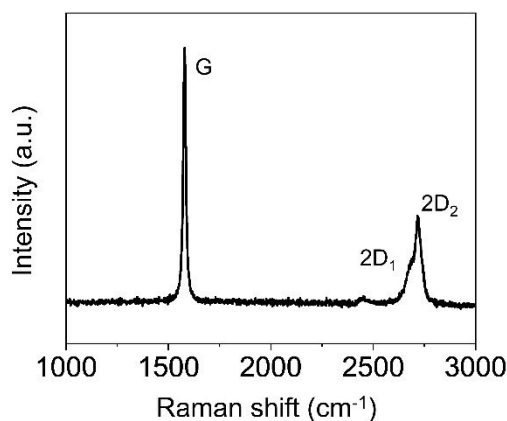


**Figure S9.** Raman spectrum of graphene covering on nichrome. The number of graphene layers is >10.

The Raman spectrum of graphene covering on nichrome shows a G peak at 1579.72 cm<sup>-1</sup>, 2D<sub>1</sub> peak at 2687.21 cm<sup>-1</sup> and 2D<sub>2</sub> peak at 2716.82 cm<sup>-1</sup>, and the 2D<sub>1</sub> and 2D<sub>2</sub> are roughly 1/4 and 1/2 the height of the G peak, respectively. Andrea studied Raman spectroscopy of graphene with different layers and graphite.<sup>11</sup> Comparing the peak shape, position and intensity of the Raman spectrum of graphene covering on nichrome with that of graphene with different layers and graphite, one can tell the layer number of graphene covering on nichrome is >10.

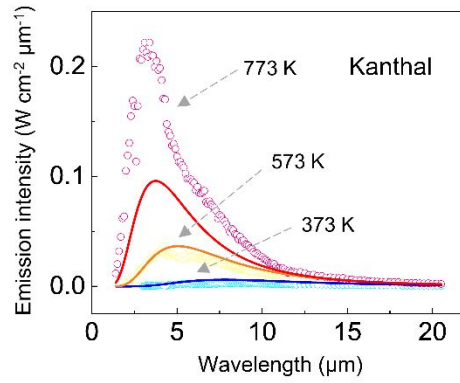


**Figure S10.** Infrared emission spectra (hollow dots) and theoretical gray-body radiation curves (solid lines) of Kanthal at 373, 573, and 773 K.

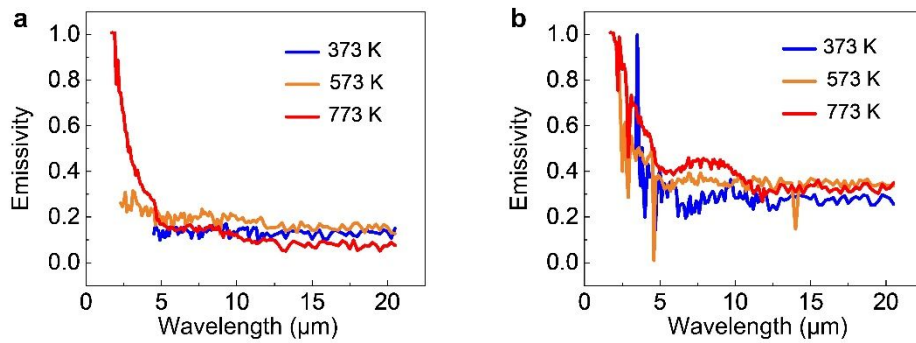


**Figure S11.** Wavelength-dependent spectral emissivity of nichrome (a) and Kanthal (b) at 373, 573 and 773 K.

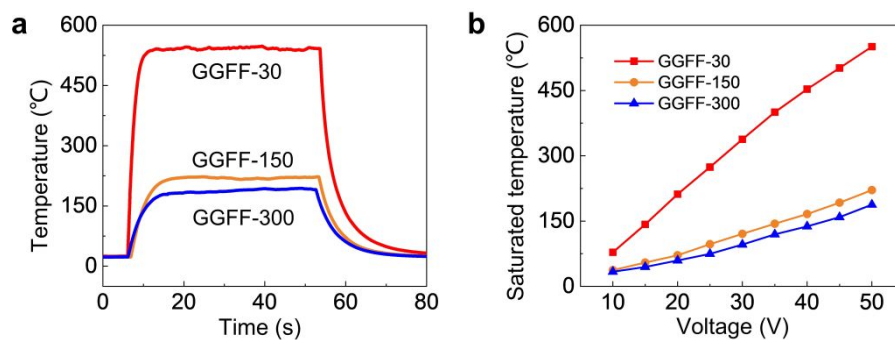


**Figure S12.** a) Temperature profiles of GGFF-30, GGFF-150, GGFF-300 under 50 V. b) Saturated temperature of GGFF-30, GGFF-150, GGFF-300 under different input voltages.

For electrothermal device, the electrical resistance influences the saturated temperature through input power:  $P = \frac{U^2}{R}$ . Therefore, the heating capability is highly dependent on the sheet resistance of GGFF. As shown in **Figure S12a**, GGFF with lower sheet resistance showed a faster electrothermal response rate (GGFF-30: 161.1 °C s<sup>-1</sup>; GGFF-150: 28.1 °C s<sup>-1</sup>; GGFF-300: 23.1 °C s<sup>-1</sup>) and higher saturated temperature (GGFF-30: 543.1 °C; GGFF-150: 221.0 °C; GGFF-300: 191.4 °C) (with input voltage of 50 V). Figure S12b presented the saturated temperature of GGFF-30, GGFF-150 and GGFF-300 at different input voltages, which showed that the saturated temperature of GGFF can be modulated by the sheet resistance and input voltage.

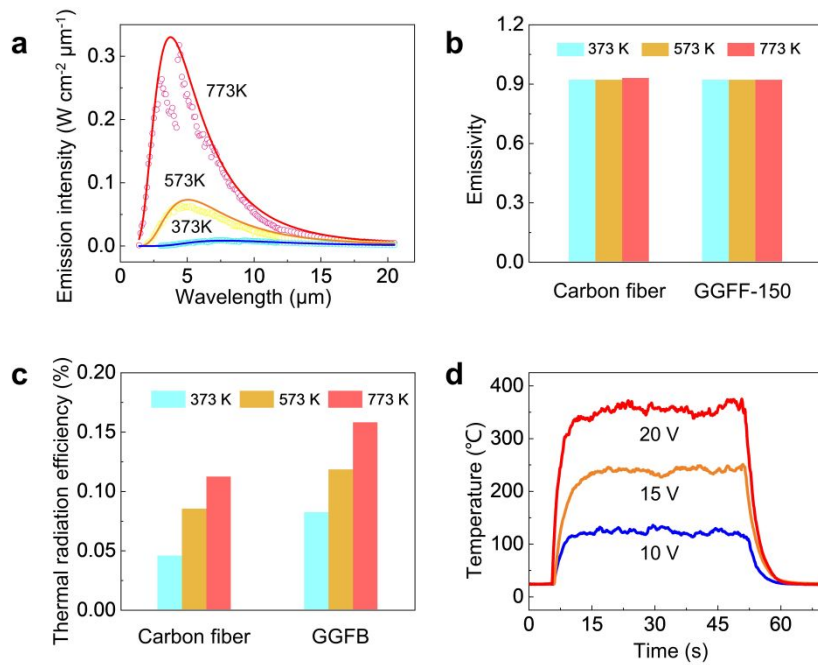


**Figure S13.** Infrared radiation property and electrothermal performances of carbon fiber. a) Infrared emission spectra of carbon fiber at 373 K, 573 K, 773 K. b) Comparisons of emissivity at 373 K, 573 K, 773 K between carbon fiber and GGFF. c) Comparisons of thermal radiation efficiency at 373 K, 573 K, 773 K between carbon fiber and GGFF. d) Temperature profiles of carbon fiber at different input voltages.

The comparisons between GGF developed in this work with the representative non-metallic heating materials, such as carbon fiber and the state-of-the-art infrared

radiation materials, for example ceramic materials were shown in **Figure S13** and **Table S2**.

The emission spectra, emissivity, thermal radiation efficiency and electrothermal response between carbon fiber and GGF were compared. As shown in Figure S13a,b, carbon fiber exhibits gray-body radiation property and has a temperature-independent emissivity, which is comparable to GGF.

But GGF showed the higher thermal radiation efficiency than that of carbon fiber (Figure S13c) (GGF: 373 K, 8.2%; 573 K, 11.8%; 773 K, 15.8%; carbon fiber: 373 K, 4.5%; 573 K, 8.5%; 773 K, 11.2%). The thermal radiation efficiency can be represented as:  $\eta = \frac{Q_r}{Q_{input}} = \frac{Q_{input} - Q_{cond} - Q_{conv}}{Q_{input}}$ , where  $Q_{input}$ ,  $Q_r$ ,  $Q_{cond}$  and  $Q_{conv}$  are input energy, heat loss due to radiation, conduction and convection, respectively. The higher thermal radiation efficiency of GGF is possibly attributed to its lower thermal conductivity than carbon fiber, which results in a less heat loss through thermal conduction. Moreover, GGF had a higher electrothermal response ( $180.0 \text{ }^\circ\text{C s}^{-1}$  at saturated temperature of  $\sim 360 \text{ }^\circ\text{C}$ ) (Figure 4c) than that of carbon fiber ( $75.0 \text{ }^\circ\text{C s}^{-1}$  at saturated temperature of  $\sim 360 \text{ }^\circ\text{C}$ ) (Figure S13d). The temperature rising rate can be represented as:  $cm \cdot \frac{dT}{dt} = Q_{input} - Q_{cond} - Q_{conv} - Q_r$ , where  $c$ ,  $m$  and  $\frac{dT}{dt}$  are specific heat capacity, mass and temperature rising rate. The less heat loss of GGF resulted in the higher temperature rising rate.

In addition, the carbon fiber usually shows the limited tunability for the electrical conductivity. The fabrication of carbon fiber always needs the carbonization process ( $1600 \text{ }^\circ\text{C}$ ) to form a turbostratic carbon phase and graphitization process ( $3000 \text{ }^\circ\text{C}$ ) to increase the ordering orientation of small turbostratic crystallites along the fiber axis<sup>12</sup>. Considering such extreme preparation conditions, it is not easy to modulate the quality of the carbon fiber, and thus the tunability of the electrical conductivity is also limited. In contrast, for GGF, glass fiber is an insulator, and the electrical conductivity of GGF is only relied on graphene, which can be modulated by layer number or crystal quality

over a wide range. For different application scenarios, the electrical conductivity can be effectively modulated by changing the CVD growth conditions of graphene, and there is no need to adjust sample size, the connection way of electrodes, or the macrostructure of materials.

Ceramic coating, such as  $\text{Fe}_2\text{O}_3$ ,  $\text{CeO}_2$ ,  $\text{MnO}_2$ , is the widely-used, state-of-the-art infrared radiation materials, which is usually prepared by blending ceramic powder, binder and deionized water, and then used as the coatings on the substrate surface through the air spraying or brushing<sup>3, 4, 13</sup>. According to the reviewer's advice, the performances of GGF and ceramic coatings were systematically compared.

The ceramic coatings used in infrared radiation usually have high emissivity and excellent high-temperature resistance (Table S2). However, the applications of ceramic coatings are limited due to the following factors: (1) low emissivity in the short waveband, (2) weak bonding strength with the substrate surface, (3) poor thermal shock resistance and (4) short working life. These drawbacks mainly result from their preparation methods. Generally, the infrared radiation coatings were used through brushing their slurry on the object's surfaces. The slurry always consists of the infrared-active powders mixed with a binder. However, the binders always lose effects under high temperature or after long-term working, and the coatings would peel off easily from the object surfaces due to the weak physical bonding between the coating and substrate. Meanwhile, the large mismatch between the thermal expansion coefficients of the coating and substrate will further aggravate the interface stability<sup>4</sup>. In addition, to realize the high and uniform infrared radiation performances, the thickness of the coating layers is usually hundreds of micrometers (it is hard to achieve uniform coating with thin brushing), which sometimes compromises the intrinsic flexibility of the substrate materials.

In our work, the CVD method was used to prepare graphene on the flexible glass fiber. The grown graphene on glass fiber is uniform and only tens of nanometers, without degrading the intrinsic flexibility of glass fiber. And because of the low

mismatch between the thermal expansion coefficients of graphene and glass fiber (glass fiber:  $5.5 \times 10^{-7} \text{ m K}^{-1}$ ; graphene:  $-2 \times 10^{-6} \text{ m K}^{-1}$ ), GGF will show superior long-term working stability. Attributed to the dual-emitter design, GGF showed a higher, temperature- and wavelength-independent emissivity (from 2.5 to 25  $\mu\text{m}$ ) than infrared radiation coatings.

## Reference

1. Muley, S. V.; Ravindra, N. M., Emissivity of Electronic Materials, Coatings, and Structures. *Jom* **2014**, *66*, 616-636.
2. Nair, R. R.; Blake, P.; Grigorenko, A. N.; Novoselov, K. S.; Booth, T. J.; Stauber, T.; Peres, N. M.; Geim, A. K., Fine Structure Constant Defines Visual Transparency of Graphene. *Science* **2008**, *320*, 1308.
3. Gahmousse, A.; Ferria, K.; Rubio, J.; Cornejo, N.; Tamayo, A., Influence of  $\text{Fe}_2\text{O}_3$  on the Structure and Near-Infrared Emissivity of Aluminosilicate Glass Coatings. *Appl. Phys. A* **2020**, *126*, 732-742.
4. Zhang, J.; Fan, X. a.; Lu, L.; Hu, X.; Li, G., Ferrites Based Infrared Radiation Coatings with High Emissivity and High Thermal Shock Resistance and Their Application on Energy-Saving Kettle. *Appl. Surf. Sci.* **2015**, *344*, 223-229.
5. Han, R.; Tariq, N. u. H.; Liu, H.; Zhao, L.; Luo, J.; Wang, J.; Cui, X.; Xiong, T., Development of High Infrared Emissivity Porous Ceramic Coating Using Pre-Synthesized Flower-Like  $\text{CeO}_2$  Powder for High Temperature Applications. *Ceram. Int.* **2022**, *48*, 1340-1348.
6. Ding, S.; Mao, J.; Zeng, X.; Cheng, X., Enhanced Infrared Emission Property of NiCr Spinel Coating Doped with  $\text{MnO}_2$  and Rare-Earth Oxides. *Surf. Coat. Technol.* **2018**, *344*, 418-422.

7. Chen, Z.; Qi, Y.; Chen, X.; Zhang, Y.; Liu, Z., Direct CVD Growth of Graphene on Traditional Glass: Methods and Mechanisms. *Adv. Mater.* **2019**, *31*, 1803639.
8. Lin, L.; Deng, B.; Sun, J.; Peng, H.; Liu, Z., Bridging the Gap between Reality and Ideal in Chemical Vapor Deposition Growth of Graphene. *Chem. Rev.* **2018**, *118*, 9281-9343.
9. Karim, N.; Zhang, M.; Afroj, S.; Koncherry, V.; Potluri, P.; Novoselov, K. S., Graphene-Based Surface Heater for De-icing Applications. *RSC Adv.* **2018**, *8*, 16815-16823.
10. Liu, G.; Shi, F.; Li Y.; Zhang Q.; Wang H., Preparation and Electrical Properties of Graphene Coated Glass Fiber Composites. *J. Inorg. Mater.* **2015**, *30*, 763-768.
11. Ferrari, A. C., Raman spectroscopy of graphene and graphite: Disorder, Electron-Phonon Coupling, Doping and Nonadiabatic Effects. *Solid State Commun.* **2007**, *143*, 47-57.
12. Frank, E.; Steudle, L. M.; Ingildeev, D.; Sporn, J. M.; Buchmeiser, M. R., Carbon Fibers: Precursor Systems, Processing, Structure, and Properties. *Angew. Chem. Int. Ed.* **2014**, *53*, 5262-5298.
13. Liu, F.; Cheng, X.; Mao, J.; Li, S.; Shao, H.; Liu, T.; Yamaguchi, T.; Zeng, X., Fabrication and Characterization of Pr<sub>6</sub>O<sub>11</sub>-HfO<sub>2</sub> Ultra-High Temperature Infrared Radiation Coating. *J. Eur. Ceram. Soc.* **2019**, *39*, 4208-4215.